DOI: 10.1021/ma100985x

Macromolecules
ARTICLE

Flow-Induced Crystallization: Unravelling the Effects of Shear Rate and Strain

Ahmad Jabbarzadeh* and Roger I. Tanner

School of Aerospace, Mechanical and Mechatronic Engineering, The University of Sydney, NSW 2006, Australia

Received May 4, 2010; Revised Manuscript Received June 14, 2010

ABSTRACT: We have used large scale nonequilibrium molecular dynamics simulations to separate the effects of shear rate ($\dot{\gamma}$) and strain (γ) in postshear crystallization of polymers. Here we show the strain plays a major role in flow-induced crystallization (FIC) and a critical strain, with a clear correlation to the rheology and molecular structure, must be applied to observe enhanced crystallization. Although the amount of crystallinity initially increases with $\dot{\gamma}$, our simulations appear to be consistent with experimental observations of an upper limit $\dot{\gamma}_c$, above which the effect is reversed, and show it is at the reciprocal of the stress relaxation time. We reveal the structural origins of this phenomenon and show the shear rate does not affect the crystallization rate in post shear crystallization of a model polymer with 162 monomers.

1. Introduction

Monatomic materials and those made of small molecules can make perfect crystals in mostly predictable structures. For most molecular materials the crystallization process is more complex and the underlying molecular structure and how fast molecules respond to kinetic and temperature changes may affect the crystallization process. Materials composed of macromolecules, such as polymers, often may form a semicrystalline rather than fully crystalline structure. Semicrystalline polymers are widely used in the polymer industry and their mechanical and physical properties strongly depend on their crystallinity and morphology. For these materials the crystallization depends on many factors including the molecular structure of the polymer, thermal history, cooling rate, presence of additives and flow conditions of the melt during processing. Polymeric materials subjected to flow show enhanced crystallization,[1] a phenomenon known as flow-induced crystallization (FIC). For simple shear, experiments[2−4] suggest that shear rate and strain jointly affect the FIC. To predict FIC using theoretical modeling,[5−7] based on deformation and rheology, a fundamental understanding of FIC is necessary. An important part of this process is to separate effects of shear rate ($\dot{\gamma}$) and total strain ($\gamma = \dot{\gamma}t$) on FIC and, to find out how these are related to rheological properties and structure during deformation, a task very difficult to achieve experimentally. Simulations,[8−15] at molecular level have helped to understand the growth mechanisms during crystallization processes. Molecular dynamics (MD),[8−14] Brownian dynamics (BD), and Langevin dynamics (LD),[15] have been used for simulations of polymer melts and solutions to gain insight at a fundamental level into the process of crystallization.

Continuum modeling of FIC has been attempted based on shear rate,[5] principal stress,[3] first normal stress difference,[4] stress relaxation,[6] and suspension theory.[7] Experiments suggest,[2] the existence of critical shear rate and strain to induce crystallization. A reversal of the effect is also reported in some experiments,[2] at high shear rates and strains. However how these phenomena relate to underlying rheology and molecular structure remains unclear. Molecular level simulations have been used,[8−15] to gain insight into polymer crystallization and to obtain valuable information.

Simulations of bulk quiescent crystallization of model polyethylene chains have been reported for stretched amorphous melts obtained from uniaxial elongation simulations.[10,11] Steady planar elongation simulations of n-eicosane at temperatures close to the melting point have shown formation of local crystalline precursor structures.[12] Molecular dynamics simulations have time and scale limitations and can simulate only very short spans of time in the order of a few tens of nanoseconds and a very small fraction of matter limited to a few thousand or at most a few million atoms.

Increasing computational power and the development of complex parallel algorithms have helped researchers to simulate crystallization for larger systems. Gee et al.[8] have recently simulated one of the largest systems to study the quiescent crystallization of a polyethylene system composed of several hundred monomers. While these works have provided valuable information on crystallization kinetics, the effects of shear rate and strain have not been explored in detail. Although experimental evidence of flow-induced crystallization is abundant in the literature, molecular simulation work in this area is scarce. Our recent simulations of alkanes of moderate length (*n*-eicosane, *n*-hexacontane) have explored, effect of steady shear on crystallization and effect of molecular size on post shear crystallization.[13] Systematic molecular dynamics simulations to separate the effects of strain and shear rate have not been attempted for larger systems due to obvious computational challenges. We now report our progress with this difficult task. We used parallel algorithms and spent many months of CPU time to conduct large scale simulations of a fairly long model polyethylene; namely *n*-dohexacontahectane $C_{162}H_{324}$ (M_w = 2273.2 g/mol), here referred to as C162 for brevity. These alkane systems are long enough to display chain folding[16,17] and often are used as ideal models of polyethylene in experiments.[18] The cooling and shear protocol (see Figure 1) used here is similar to that of a typical shear-induced crystallization experiment, where a melt, heated to a high temperature, is cooled to a crystallization temperature, and then is subjected to a step shear for a short time, and then is allowed to crystallize at rest.

*Corresponding author. E-mail: ahmadj@aeromech.usyd.edu.au.

 Published on Web 09/02/2010

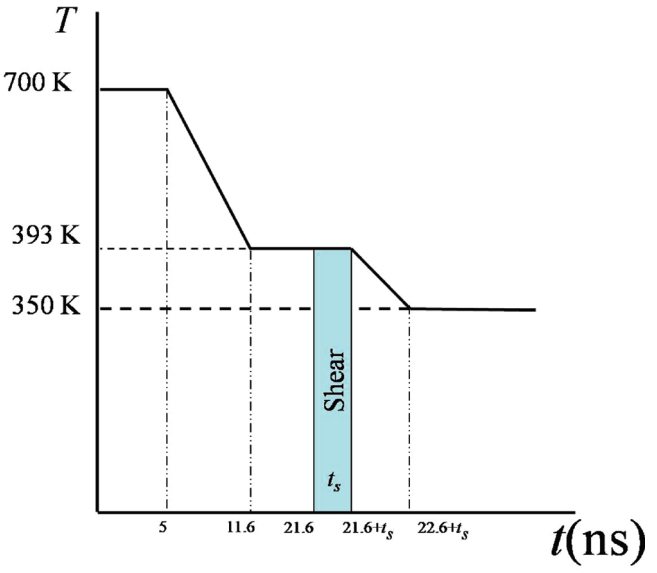

Figure 1. Temperature profile during shearing and cooling stages for the shear-induced crystallization simulations.

2. Simulation Methods

2.1. Molecular Model. We are using a united atom model in which CH_2, and CH_3 groups are treated as single interaction sites. We simulate a total number of 686 C162 molecules (111132 united atoms).The molecular model includes bonded valence interactions (including stretching, angle and torsion) and is due to Siepmann and co-workers.[19] The potential parameters are given elsewhere.[20] For nonbonded van der Waals interactions we are using a 6−12 Lennard-Jones potential. We have used the Weeks−Chandler−Andersen (WCA)[21] version of a shifted Lennard-Jones potential with a cut off distance of $r_c = 0.43$ nm. This potential is purely repulsive and has no attractive tail and is suitable for simulation of liquid and solid phases and has the benefit of reducing the computational effort. It is shown that at reduced densities above 0.65 (~250 kg/m^3 for our system), the repulsive forces largely determine the equilibrium structure and behavior of the fluid.[21] It is however essential to make proper corrections to pressure to account for the cutoff. Applying these corrections, our own *NPT* simulations, using a larger cut off at $r_c = 1$ nm (2.5 σ), confirm this, showing the calculated density at $T = 700$ K and $P = 1$ atm is only different by 1 kg/m^3, which is within the statistical uncertainty. For other structural properties, such as radius of gyration and end-to-end distance, we also find similar results. A simulation for a semicrystalline system at 350 K also found the density was lower for the repulsive potential by only 2%.

The isobaric−isothermal (*NPT*) version of the SLLOD algorithm[22] was used for our crystallization simulations. Constant pressure simulations realistically allow the system to contract to the state point corresponding to the final density and temperature. The SLLOD[22] equations of motion given by eq 1 govern motion of united atoms in the constant pressure simulations

$$\dot{\mathbf{r}}_i = \frac{\mathbf{p}_i}{m_i} + \mathbf{e_x}\dot{\gamma} r_{zi} + \dot{\varepsilon}\mathbf{r}_i$$
$$\dot{\mathbf{p}}_i = \mathbf{F}_i - \mathbf{e_x} p_{zi}\dot{\gamma} - \zeta \mathbf{p}_i - \dot{\varepsilon}\mathbf{p}_i$$
$$\dot{V} = 3\dot{\varepsilon} V \qquad (1)$$

Here $\mathbf{e}_x$ is the unit vector in x direction (flow direction), $\dot{\gamma}$ is the shear rate; $\mathbf{r}_i$, $\mathbf{p}_i$, and m_i are position vector, peculiar momenta, and mass of atom i. $\mathbf{F}_i$ is the total force applied by all other atoms in the system on atom i. Coefficient ζ is the Gaussian thermostat given by eq 2:

$$\zeta = \frac{\sum_{i=1}^{N} (\mathbf{F}_i.\mathbf{p}_i - \dot{\gamma} p_{xi} p_{zi})}{\sum_{i=1}^{N} \mathbf{p}_i^2} \qquad (2)$$

V is the volume of the simulation box. Dynamics of the simulation box volume V given in eq 1, is governed by the dilation rate ε, which itself is calculated by integrating eq 3

$$\ddot{\varepsilon} = \frac{(P - P_0)V}{QNk_B T} \qquad (3)$$

where P and P_0 are the instantaneous pressure and the target pressure. Q, N, k_B, and T are the damping constant, total number of atoms, Boltzmann constant, and temperature. Here ε the dilation rate of the simulation box is implemented with a Nosé−Hoover feedback scheme which implies that the instantaneous pressure will fluctuate about a mean value of P_0.The pressure is calculated by eq 4 using the trace of stress tensor. Long range corrections,[23] are applied to account for the cutoff effect of the Lennard-Jones potential.

$$P = -\frac{1}{3}(\sigma_{xx} + \sigma_{yy} + \sigma_{zz}) \qquad (4)$$

The elements of stress tensor are calculated by the Irving−Kirkwood[24] method given by eq 5:

$$\sigma_{\alpha\beta} = -\frac{1}{V}\langle \sum_{i}^{N} m_i u_{i\alpha} u_{i\beta} + \sum_{i}^{N}\sum_{j>i}^{N} r_{ij\alpha} F_{ij\beta} \rangle \qquad (5)$$

The first sum in the right-hand side of eq 5 is the kinetic contribution where α and β are coordinate system axes which for a Cartesian system can be simply substituted by X, Y, or Z, and $u_{i\alpha}$ and $u_{i\beta}$ are the peculiar velocity components of particle i in α and β directions. The second sum represents the configuration or potential contribution where $r_{ij\alpha}$ is the α component of the distance vector between particles i and j and $F_{ij\beta}$ is the β component of the force exerted on particle i by particle j.

For *NVT* simulation the equations of motion are the same as given by eq 1, without the terms involving ε and last line in the equations set (V is constant). Periodic boundary conditions in all three directions are applied for quiescent simulations. Lees−Edwards sliding brick periodic boundary conditions,[25] are applied for planar shear simulations. Equations of motion are integrated by a leapfrog version of the Verlet algorithm with a time step of 4.709 fs. Domain decomposition parallel simulations,[20] algorithm with good efficiency was used for all calculations.

The first normal stress difference is calculated from the normal stresses using the following equation:

$$N_1 = \sigma_{xx} - \sigma_{zz} \qquad (6)$$

2.2. Degree of Crystallinity and Structural Properties. To quantify the crystallinity, following our previous studies,[13] of C20 and C60 crystallization, we used the chord order parameter g_2. We have shown this is a more accurate measure of crystallinity content than that inferred from the density (dilatometry techniques).[13] The second and fourth rank correlation functions,[26,27] g_2 and g_4 given by eqs 7

$$g_2(\Gamma) = \langle \cos 2(\theta_{ij}) \rangle_{i,j}, \quad g_4(\Gamma) = \langle \cos 4(\theta_{ij}) \rangle_{i,j} \qquad (7)$$

detect the crystallinity from parallel alignment of the chord vectors that connect every other pair of united atoms along the backbone of the molecule. Here θ_{ij} is the angle between a pair of chord vectors i and j. The $\langle\rangle_{i,j}$ bracket denotes averaging over time and pairs of chord vectors and $\mathbf{\Gamma}$ is the spatial domain over which g_2 and g_4 are calculated. We calculate $g_2(\mathbf{\Gamma})$ by averaging over $i-j$ chord pairs for which the position of j chord is in a sphere, of 1.2 nm diameter, whose center lies on the position of chord i, followed by averaging over all i. Considering the C−C bond length of 0.153 nm and C−C−C bond angle of 114° that we have used in our model this is a sphere with a diameter of about 5 times the chord length. The parallel alignment of chord vectors contributes positively to both g_2 and g_4. That is, values close to 1 for both g_2 and g_4 indicate the chord vectors are aligned parallel to each other. So $g_2 \approx g_4 \approx 1$ corresponds to parallel alignment of the chord vectors and full crystallinity. We have not reported g_4 in the results as in all cases here $g_4 \sim g_2$.

We have also calculated the radius of gyration for the molecules from the following expression:

$$\langle R_g{}^2 \rangle = \left\langle \frac{\sum_i m_i |\mathbf{r}_i - \mathbf{r}_{cm}|^2}{\sum_i m_i} \right\rangle \tag{8}$$

where m and $\mathbf{r}$ are the mass and position of each atom on the molecule and $\mathbf{r}_{cm}$ is the center of mass of the molecule.

We have also calculated the order tensor[28] $\mathbf{S}$ given as

$$\mathbf{S} = \frac{3}{2}\left\langle \frac{1}{N}\sum_{i=1}^{N}\left(\mathbf{u}_i\mathbf{u}_i - \frac{1}{3}\mathbf{I}\right)\right\rangle \tag{9}$$

where $\mathbf{u}_i$ is the unit vector along the longest axis of inertially equivalent ellipsoid for the molecule and $\mathbf{I}$ is the unit tensor. The longest semiaxis is the eigenvector corresponding to the smallest eigenvalue of the inertia tensor of the molecules. The order tensor is a traceless tensor and its largest eigenvalue is called the order parameter S. The molecular order parameter S, can be any number between 0 (perfect disorder) and 1 (perfect order).

2.3. Post-Shear Crystallization Protocol. To separate the effects of shear rate and strain on the post shear crystallization we have used a protocol which is similar to that used in experiments. Figure 1 show the temperature profile and during cooling and shear application for all the simulations conducted here.

To generate the initial configuration of the melt, a constant volume (NVT) simulation was started at a lower density and at a constant temperature of $T = 700$ K and then was allowed to equilibrate for 5 ns. This temperature is well above the melting temperature of C162 of $T_m = 397.5$ K.[30] The generated configuration was then equilibrated for another 5 ns at constant temperature and pressure of 700 K and 1 atm. The NPT simulation at 700 K and 1 atm produced an amorphous melt with calculated ratio of mean square end-to-end distance to the mean-square of the radius of gyration, $\langle R^2_e\rangle/\langle R^2_g\rangle = 5.56$, close to that of a Gaussian chain configuration (∼6)[29] and a density of 705 kg/m^3. The annealed melted system of 700 K was then cooled by 50 K steps, to a crystallization temperature $T_c = 393$ K, while being allowed to equilibrate for 1.1 ns at each cooling step. We chose $T_c = 393$ K, as it is shown,[30] the crystallization rate is the highest in the range close to the melting point. The melt was then equilibrated for another 10 ns after the temperature reached 393 K. On completion of this stage the system was still amorphous (shown in Figure 2) with a density of 815 kg/m^3.

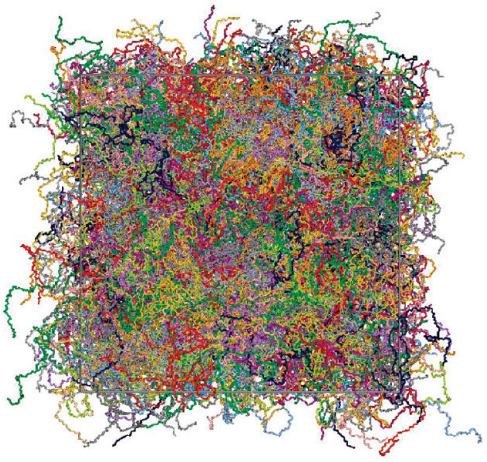

Figure 2. Snapshot of the fully amorphous C162 melt at $T = 393$ K and $P = 1$ atm.

We used the equilibrated melt configuration at $T = 393$ K for all the subsequent planar Couette shear simulations. In this stage the shearing was continued at a certain $\dot{\gamma}$ until a prescribed total strain was applied. After the cessation of shearing the melt was cooled further to 350 K at a cooling rate of 10 K per 0.235 ns and then allowed to crystallize at rest for extended times of up to 63 ns. Experiments on C162 have shown a linear relation between the degree of undercooling and crystallization rate.[30] The undercooling was necessary to observe meaningful crystallization during the short time scales achievable by our MD simulations. The model has been shown in our earlier work,[13] to overestimate the melting temperature of short alkane by ∼10 K, and our undercooling of 50 K is conservatively chosen to account for this.

3. Results and Discussion

In parts a and b of Figure 3, we present snapshots of a system which had been subjected to planar Couette shear at $\dot{\gamma} = 10^9$ s^{-1} for a total strain of $\gamma = 5$ and then was allowed to crystallize for 58 ns, reaching 58% crystallinity. In the semicrystalline structure shown in Figure 3b, two distinct lamellae can be seen with a mixture of extended, once and twice folded chains which often occupied both lamellae. A fully extended all trans C162 is ∼20.66 nm long. We calculate the thickness of each lamella to be about ∼7.5 nm which is expected, due to folding. Between the two lamellae we measure a ∼37° splaying angle which is also observed in experiments,[30] and is suggested to be the early stages of spherulite formation through a ciliation mechanism,.[30] In Figure 4, we present snapshots of crystallization stages of a melt which had been presheared at a shear rate of 1.78×10^8 s^{-1} for a total strain of $\gamma = 5$, and then was allowed to crystallize at rest. In these snapshots the chains are shown in full by application of periodic boundary conditions to the center of mass of the molecule, to allow for better visualization of individual chains during crystallization.

3.1. The Effect of Shear Rate on FIC. In Figure 5 we have plotted crystallinity versus time for melts presheared at shear rates in the range of $\dot{\gamma} = 10^8 - 10^{10}$ s^{-1}. To isolate the effect of the shear rate all systems have been subjected to the same total strain of $\gamma = 5$ during preshearing process. It is striking that despite 2 orders of magnitude change in $\dot{\gamma}$ the crystallization rate is not affected much. To compare the effect of shear rate on crystallinity developed over a certain amount of time we have plotted g_2 as a function of shear rate in Figure 6. This figure shows crystallinity after 30 ns, varies by only ∼10% within the examined shear rates. Interestingly,

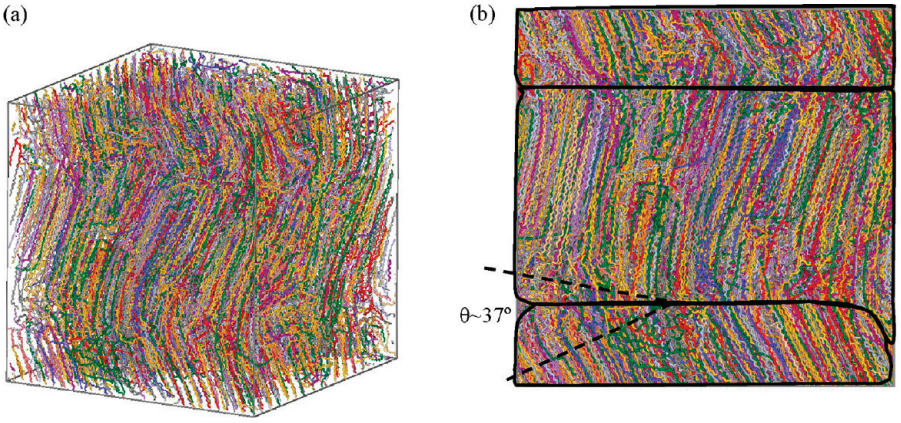

Figure 3. (a) Snapshot of a system presheared at $\dot{\gamma} = 10^9\ s^{-1}$, for a total strain of $\gamma = 5$ then allowed to crystallize at 350 K for 58 ns; (b) same as part a, shown in the *YZ* (gradient−vorticity) plane. The thick lines show the approximate boundaries of the two distinct lamellae formed, and the splaying angle $\theta = 37°$ is the angle between the normals to the surface of the two lamellae.

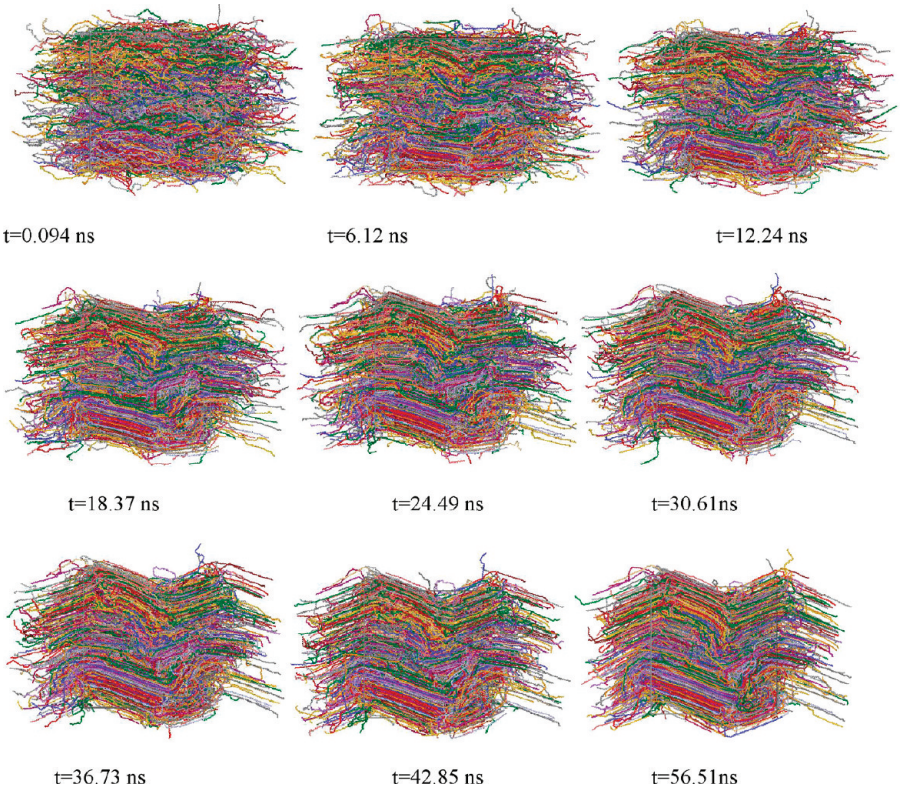

Figure 4. Snapshots of crystallization stages of C162 melt which was subjected to preshearing at a shear rate of $1.78 \times 10^8\ s^{-1}$. The snapshots are shown in the *YZ* (gradient−vorticity) plane. Molecules are shown by different colors to enhance visualization.

crystallinity initially increases with the shear rate up to $3.162 \times 10^8\ s^{-1}$, and then drops as $\dot{\gamma}$ is increased further. The results here suggest although the final crystallinity increases initially with the shear rate there is a critical shear rate above which the effect is reversed. The reversal of the effect at higher shear rates is in agreement with experiments of Bove and Nobile.[2] We did not detect the lower limit of shear rate, for onset of flow-induced crystallization and this shear rate is possibly lower than those examined in our simulations.

3.2. Effect of Shear Strain on FIC. To examine the effect of only the strain we subjected the melt to the same shear rate of $10^9\ s^{-1}$, applying a number of different strains, and then allowed it to crystallize. The crystallinity versus time is shown for these systems in Figure 7. Here, $\gamma = 0$ represents the melt, which followed the same temperature profile shown in Figure 1 without application of shear. It is striking that both the amount of crystallinity (see the inset in Figure 7) and the rate of crystallization change significantly with γ. No meaningful crystallization increase was observed at the lowest strain of $\gamma = 1$, despite a slight increase in crystal content compared to the nonsheared system ($\gamma = 0$). The crystallization begins at $\gamma = 2$, and then as the strain is increased to $\gamma = 3$, a noticeable change in the slope marks an increase in the rate of crystallization. Clearly a strain, in the range of $1 < \gamma < 2$, was needed to induce crystallization. The inset in Figure 7 shows initially a sharp increase in the final crystallinity as the strain is increased, followed by a plateau at higher strains. This is in agreement with experimental[4] and modeling[3] results, which showed a limiting effect of strain. Reversal of the effect, as reported by Bove and Nobile,[2] was not detected although it could not be ruled out, as we did not go beyond $\gamma = 10$. From Figure 7, we clearly see the

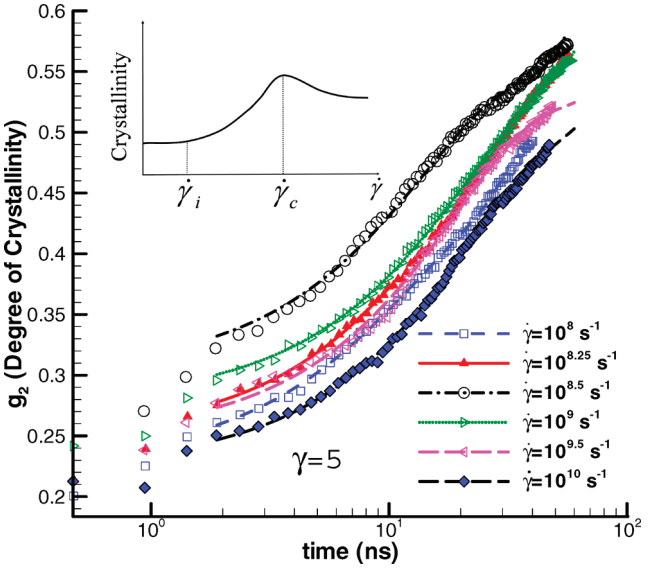

Figure 5. Degree of crystallinity (g_2) versus time during crystallization of C162 at 350 K. Before cooling to 350 K, each system was presheared at 393 K for a total strain $\gamma = 5$, at a different shear rate as shown. The lines are third order polynomial fit to data after the temperature is reached 350 K. The inset at the top shows the proposed effect of shear rate where $\dot{\gamma}_i$, is the induction shear rate and, $\dot{\gamma}_c$ is the critical shear rate.

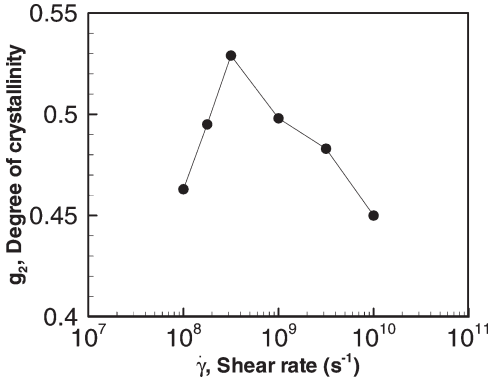

Figure 6. Degree of crystallinity (g_2) versus shear rate for postshear crystallization of C162 at 350 K, after 30 ns of crystallization time. All systems are sheared for a total strain of $\gamma = 5$.

crystallization rate is the largest at $\gamma \sim 2-3$. Strain-induced crystallization behavior seen here was independent of the shear rate and a similar behavior was observed at a higher shear rate of 10^{10} s^{-1} and also a lower shear rate of 10^8 s^{-1} (results not shown). That is the critical strain to induce crystallization was unchanged for the range of shear rates we examined here.

4. Rheology, Structure, and Discussion

To connect our observations to rheology and structure, in Figure 8 we have plotted the shear stress, crystallinity and molecular order,[31] S, as a function of strain during shearing process at different shear rates. The shear stress (σ_{xz}) is calculated using eq 5. At the onset of shearing, in Figure 8, we see a clear stress overshoot which increases with $\dot{\gamma}$. Occurrence of this stress overshoot, which decays to a steady state at higher strains, is well-known for polymers. The magnitude of stress overshoot increases with $\dot{\gamma}$ and length of molecules,.[32] Fitting the data to third order polynomial, we find that the maximum shear stress occurs at critical strains of $\gamma_c^{\sigma_{xz,max}} = 2, 2.1, 2.3, 2.27$, and 2.4 respectively for $\dot{\gamma} = 10^8$, 3.162×10^8, 10^9, 3.162×10^9, and 10^{10} s^{-1}. Our results

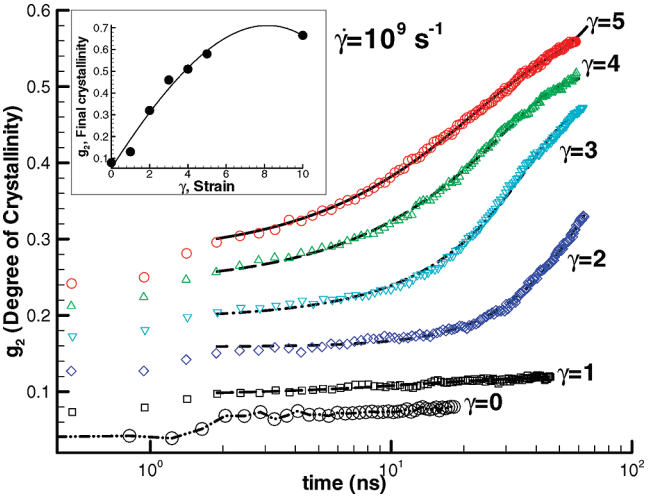

Figure 7. Degree of crystallinity (g_2) versus time during crystallization of C162 as the temperature is dropped from 393 to 350 K and allowed to crystallize. Before cooling, each system was subjected to the same shear rate of 10^9 s^{-1} but sheared for a different total strain as shown. The lines (for $\gamma = 1-5$) are third order polynomial fit to data after the temperature is reached 350 K. The inset shows the final crystallinity as a function of strain.

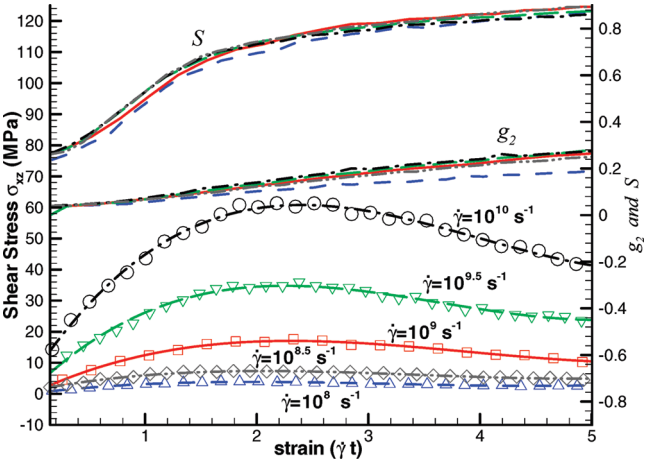

Figure 8. Shear stress (σ_{xz}, lines with symbols), degree of crystallinity (g_2, lines), and molecular order parameter (S, lines) as a function of strain ($\gamma = \dot{\gamma}t$) during preshearing process for various shear rates, 10^8 (dashed line), 3.162×10^8 (dash-dot-dot line), 10^9 (solid line), 3.162×10^9 (long dashed line) and 10^{10} s^{-1} (dash−dot line).

suggest $\gamma_c^{\sigma_{xz,max}}$ being mostly independent of $\dot{\gamma}$ in agreement with an extended Doi−Edwards model.[33] This critical strain is close to $\gamma_c \sim 2$, needed for the start of FIC in the melt presheared at $\dot{\gamma} = 10^9$ s^{-1} (Figure 7). Such stress overshoot at $\gamma_c \sim 2$ is also reported,[3] in FIC simulations of large aspect ratio dumbbell models of isotactic polypropylene (iPP). Experiments[2] with isotactic poly(1-butene) (i-PB) imply $\gamma_c \sim 2$ for melts sheared at $\dot{\gamma} > 0.01$ s^{-1}. We have plotted the first normal stress difference (N_1) in Figure 9 as a function of strain during the shearing process, and similar to Figure 8, we have included the S and g_2. In this plot, we can see the peak in the first normal stress difference, N_1, takes place at $\gamma \sim 3.5$. This is consistent with earlier simulation of C100 where the peak was observed at a similar strain independent of the shear rate. Given the critical strain of $\gamma_c \sim 2$ is close to the peak observed in the shear stress, than that is seen for the first normal stress difference, we postulate shear stress to be a better indication of critical strain for shear-induced crystallization. In Figure 8, the shear stress peaks when S almost

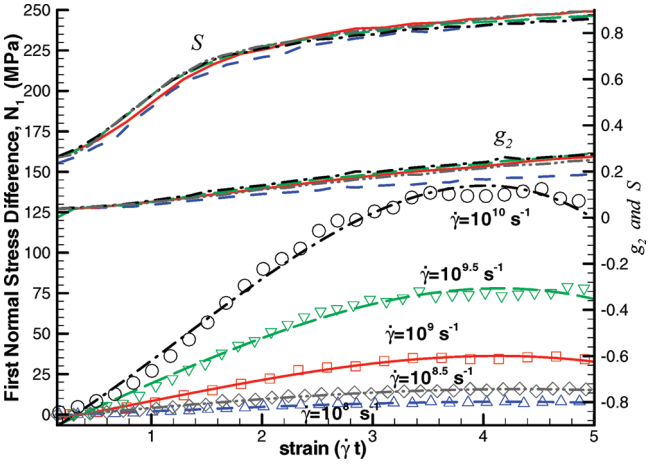

Figure 9. First normal stress difference (N_1, lines with symbols), degree of crystallinity (g_2, lines), and molecular order parameter (S, lines) as a function of strain ($\gamma = \dot{\gamma}t$) during preshearing process for various shear rates, 10^8 (dashed line), 3.162×10^8 (dash−dot−dot line), 10^9 (solid line), 3.162×10^9 (long dashed line), and 10^{10} s^{-1} (dash−dot line).

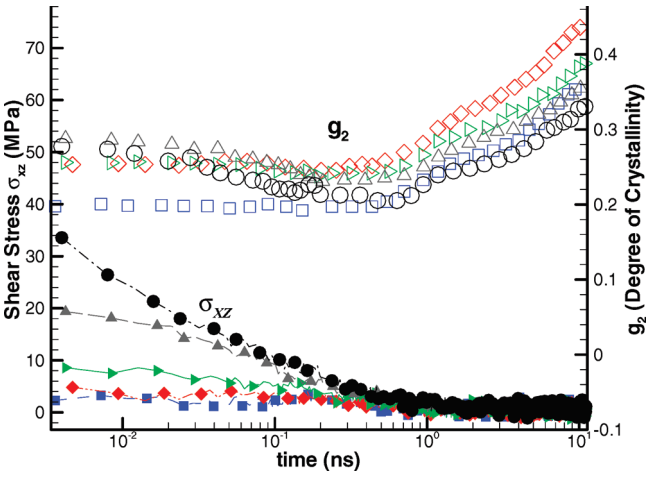

Figure 10. Shear stress σ_{xz} (filled symbols) and degree of crystallinity g_2, (open symbols), immediately after the cessation of shear and application of total strain $\gamma = 5$ for C162 at various shear rates 10^8 (blue box), 3.162×10^8 (red tilted square), 10^9 (green sideways triangle), 3.162×10^9 (purple triangle pointing up), and 10^{10} s^{-1}(black circle).

reaches a plateau after a sharp ascent to its climax. The molecular order parameter, S, is almost insensitive to the range of $\dot{\gamma}$ we examined here and is mostly dependent on the strain. The increase in crystallinity (g_2), during preshearing, is small but noticeable. There is a consistent increase in g_2 with both $\dot{\gamma}$ and γ, with strain having a larger effect. At $\gamma = 5$, we find $g_2 \sim 0.19$, 0.25, 0.26, 0.28, and 0.28, respectively, for $\dot{\gamma} = 10^8$, 3.162×10^8, 10^9, 3.162×10^9, and 10^{10} s^{-1}. The initial crystallinity and order built into the melt during shearing is crucial for further crystallization. Since $\dot{\gamma}$ makes only a small difference in S and g_2 (see Figure 8) the crystallization that follows also shows only small differences (Figure 5). Despite this small difference, one would expect the crystallinity to increase with $\dot{\gamma}$, as g_2 consistently increases with $\dot{\gamma}$ during shearing. However the results in Figure 5 suggest otherwise, as we find the crystallinity initially increases with $\dot{\gamma}$ reaching a peak at $\dot{\gamma} = 3.16 \times 10^8$ s^{-1} and then drops as shear rate is increased further. Interestingly, for $\dot{\gamma} = 10^{10}$ s^{-1}, the final crystallinity is even lower than that for $\dot{\gamma} = 10^8$ s^{-1}. The origin of an upper limit in the effect of $\dot{\gamma}$ on FIC emerges from Figure 10 which shows shear stress and g_2 against time in the early stages just after the cessation of shear. We can clearly see a

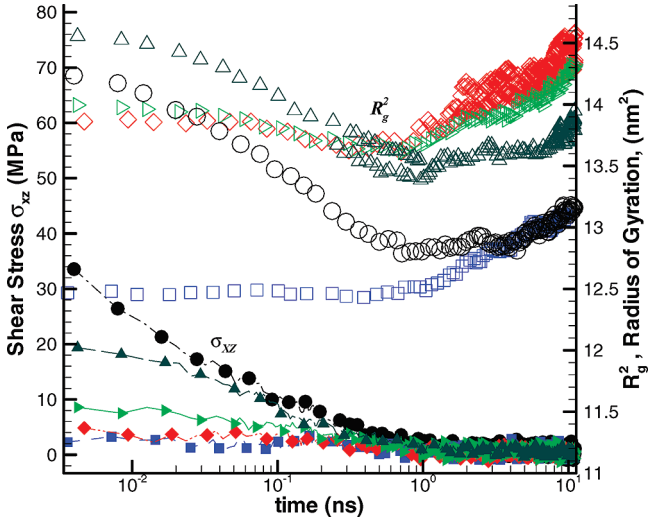

Figure 11. Shear stress σ_{xz} (filled symbols) and square radius of gyration R_g^2, (open symbols), immediately after the cessation of shear and application of total strain $\gamma = 5$ for C162 at various shear rates 10^8 (blue box), 3.162×10^8 (red tilted square), 10^9 (green sideways triangle), 3.162×10^9 (purple triangle pointing up), and 10^{10} s^{-1}(black dot).

noticeable loss of crystallinity, right after the cessation of shear and as the shear stress relaxes, for melts sheared at $\dot{\gamma} > 3.16 \times 10^8$ s^{-1}. The loss is proportional to the shear rate. Note, at $\dot{\gamma} = 10^{10}$ s^{-1}, that g_2 drops to the same level or even lower than that for 10^8 s^{-1}. The loss in crystallinity is due to recoiling which is proportional to the stress and hence the shear rate. This recoiling effect can be seen more clearly in Figure 11 where the time average square radius of gyration $\langle R_g^2 \rangle$ is plotted as a function of time, immediately after the cessation of shear. Here again we see the dramatic drop in radius of gyration for $\dot{\gamma} = 10^{10}$ s^{-1}.

From Figure 10, we estimate the stress relaxation time $\lambda \approx 3$ ns. The maximum flow-induced crystallinity was achieved at $\dot{\gamma} \sim 3.16 \times 10^8$ s^{-1}, which is close to the reciprocal stress relaxation time, $1/\lambda \approx 3.3 \times 10^8$ s^{-1}. At this critical shear rate of $\dot{\gamma}_c \approx 1/\lambda$ the flow-induced crystallization is the maximum, and for $\dot{\gamma} < \dot{\gamma}_c$ the shear rate positively affects the crystallization. For $\dot{\gamma} > \dot{\gamma}_c$ the effect of the shear rate on post shear crystallization is reversed due to recoiling effect. The inset at the top corner of Figure 5 shows our proposed effect of shear rate on FIC, which is characterized by the induction shear rate $\dot{\gamma}_i$ above which FIC begins, and $\dot{\gamma}_c$ at which the crystallization peaks and above which the effect is reversed. We have not explored the induction shear rate ($\dot{\gamma}_i$), for C162 at this particular strain ($\gamma = 5$); however, we estimate it to be $\dot{\gamma}_i < 10^8$ s^{-1}, which is beyond that achievable by our current MD simulations.

Experimental evidence of upper limit of shear rate on FIC is reported for high molecular weight isotactic poly(1-butene) (i-PB) by Bove and Nobile.[2] They have reported a critical strain at a given $\dot{\gamma}$, and an induction shear rate of $\dot{\gamma}_i \approx 0.01$ s^{-1} for $\gamma \sim 5$. A critical shear rate of $\dot{\gamma}_{c,iPB} \sim 0.05-0.1$ s^{-1} can be inferred from their results, which agrees with our conjecture, considering stress relaxation time for i-PB to be, $\lambda_{iPB} \approx 10-100$ s.[34] Modeling and experimental works,[3,4] on iPP, sheared at $\dot{\gamma} < 100$ s^{-1}, suggest the crystallization increases with $\dot{\gamma}$ and the onset of FIC to be at $\dot{\gamma}_i \sim 1$ s^{-1}. Stress relaxation time for iPP melt is reported,[35,6] to be in the order of $\lambda_{iPP} \approx 0.01-0.001$ s and this puts $\dot{\gamma}_{c,iPP} = 1/\lambda_{ipp} \approx 100-1000$ s^{-1}, which is higher than those examined in these works,.[3,4] We think exploring this high shear rate region should reveal the limiting effect of the shear rate in postshear crystallization of iPP and corresponding, $\dot{\gamma}_{c,iPP}$.

FIC experiments on a variety of polymers including bimodal HDPE by Balzano,[36] have shown the crystallization rate to be

independent of shear rate, and the increase in the onset temperature to be mostly dependent on strain. These polymers have much larger molecular weights and are subjected to much lower shear rates ($1-200\ s^{-1}$) than those in our simulations. However Weissenberg numbers in our simulations ($Wi = \lambda\dot{\gamma} \approx 0.03-3$) are comparable to those in Balzano's experiments of $Wi = \lambda\dot{\gamma} \approx 0.07-14$ (assuming $\lambda \approx 0.07$ s for HDPE[37]).

5. Conclusion

Experimental and modeling works have shown the combined role of shear rate and strain on FIC. Through atomistic level simulations, we have unambiguously shown that the onset of FIC is at a critical total strain γ_c which coincides with a peak in the shear stress overshoot ($\sigma_{xz,max}$) and significant molecular orientational order (S). We show that the final crystallinity increases with the total strain, and postulate that, at $\gamma \approx \gamma_c$ the crystallization rate is the maximum. Given the difficulty in detecting molecular order during the flow, monitoring the shear stress presents itself as a practical method to quantify γ_c for a specific polymer. Given the similarity of critical strain, obtained in our simulations, the experiments,[2] and modeling,[3] $\gamma_c \sim 2-3$ may be a universal value independent of the polymer type, provided $\dot{\gamma} > \dot{\gamma}_i$. We have confirmed the existence of a limiting shear rate, seen in the experiments, and clearly resolved its origins. Stress relaxation time (λ), can be used to quantify this limiting critical shear rate $\dot{\gamma}_c \approx 1/\lambda$ at which maximum crystallinity may achieve for a certain strain. For high molecular weight polymers $\dot{\gamma}_c$ is at lower shear rates and is more likely to be encountered during processing. We expect at higher total strains or at lower temperatures during preshearing the recoiling effect to be less severe, making the peak crystallinity at $\dot{\gamma}_c$ less pronounced.

Acknowledgment. We gratefully acknowledge the support of this study by Australian Cooperative Research Centre for Polymers, and also an Australian Research Council (ARC) Discovery Grant. We also thank the Australian Centre of Advanced Computing and Communications and also Australian National Computational Infrastructure Facility for the generous time allocated for computing.

References and Notes

(1) Binsbergen, F. L. Orientation-induced Nucleation in Polymer Crystallization. *Nature* **1966**, *211*, 516–517.
(2) Bove, L.; Nobile, M. R. Shear-induced crystallization of isotactic poly(1-butene). *Macromol. Symp.* **2002**, *185*, 135–147.
(3) Zheng, R.; Kennedy, P. K. A model for post-flow induced crystallization: General equations and predictions. *J. Rheol.* **2004**, *48*, 823–842.
(4) Koscher, E.; Fulchiron, R. Influence of shear on polypropylene crystallization: Morphology development and kinetics. *Polymer* **2002**, *43*, 6931–6942.
(5) Braun, J.; Wippel, H.; Eder, G.; Janeschitz-Kriegl, H. Industrial Solidification Processes in Polybutene-1 Part Il-Influence of Shear Flow. *Polym. Eng. Sci.* **2003**, *43*, 188.
(6) Guo, J.; Narh, K. A. Computer simulation of stress induced crystallization in injection molded thermoplastics. *Poly. Eng. Sci.* **2001**, *41*, 1996–2012.
(7) Dai, S.-C.; Qi, F.; Tanner, R. I. Strain and strain-rate formulation for flow-induced crystallization. *Polym. Eng. Sci.* **2006**, *46*, 659–669.
(8) Gee, R. H.; Lacevic, N.; Fried, L. E. Atomistic simulations of spinodal phase separation preceding polymer crystallization. *Nat. Mater.* **2005**, *5*, 39–43.
(9) Fujiwara, S.; Sato, T. Molecular dynamics simulation of structural formation of short polymer chains. *Phys. Rev. Lett.* **1998**, *80*, 991–995.
(10) Ko, M. J.; Waheed, N.; Lavine, M. S.; Rutledge, G. C. *J. Chem. Phys.* **2004**, *121*, 2823.
(11) Koyama, A.; Yamamoto, T.; Fukao, K.; Miyamoto, Y. *J. Chem. Phys.* **2001**, *115*, 560.
(12) Ionescu, T. C.; Baig, C.; Edwards, B. J.; Keffer, D. J.; Habenschuss, A. *Phys. Rev. Lett.* **2006**, *96*, 037802.
(13) Jabbarzadeh, A.; Tanner, R. I. Crystallization of alkanes under quiescent and shearing conditions. *J. Non-Newtonian Fluid Mech.* **2009**, *160*, 11–21.
(14) Waheed, N.; Lavine, M. S.; Rutledge, G. C. Molecular simulation of crystal growth in n-eicosane. *J. Chem. Phys.* **2002**, *116*, 2301–2309.
(15) Dukovski, I.; Muthukumar, M. Langevin dynamics simulations of early stage shish-kebab crystallization of polymers in extensional flow. *J. Chem. Phys.* **2003**, *118*, 6648–6655.
(16) de Silva, D. S. M.; Zeng, X. B.; Ungar, G.; Spells, S. J. *J. Macromol. Sci. B* **2003**, *B42*, 915–927.
(17) Ungar, G.; Stejny, J.; Keller, A.; Bidd, I.; Whiting, M. C. The Crystallization of Ultralong Normal Paraffins: The Onset of Chain Folding. *Science* **1985**, *229*, 386–389.
(18) Winkel, A. K.; Hobbs, J. K.; Miles, M. J. Annealing and melting of long-chain alkane single crystals observed by atomic force microscopy. *Polymer* **2000**, *41*, 8791–8800.
(19) Siepmann, J. I.; Martin, M. G.; Mundy, C. J.; Klein, M. L. Intermolecular potentials for branched alkanes and the vapour-liquid phase equilibria of n-heptane, 2-methylhexane, and 3-ethylpentane. *Mol. Phys.* **1997**, *90*, 687–693.
(20) Jabbarzadeh, A.; Atkinson, J. D.; Tanner, R. I. A parallel algorithm for molecular dynamics simulation of branched molecules. *Comput. Phys. Commun.* **2003**, *150*, 65–84.
(21) Weeks, J. D.; Chandler, D.; Andersen, H. C. *J. Chem. Phys.* **1971**, *54*, 5237–5247.
(22) Daivis, P. J.; Evans, D. J. Comparison of constant pressure and constant volume nonequilibrium simulations of sheared model decane. *J. Chem. Phys.* **1994**, *100*, 541–547.
(23) Allen, M. P.; Tildesley, D. J. *Computer simulation of liquids*: Clarendon Press: Oxford, U.K., 1987.
(24) Irving, J. H.; Kirkwood, J. G. The statistical mechanical theory of transport processes. IV. The equations of hydrodynamics. *J. Chem. Phys.* **1950**, *18*, 817–829.
(25) Lees, A. W.; Edwards, S. F. The computer study of transport processes under extreme conditions. *J. Phys.C* **1972**, *5*, 1921–1928.
(26) Frenkel, D.; Eppenga, R. Evidence for algebraic orientational order in a two-dimensional hard-core nematic. *Phys Rev A* **1985**, *31*, 1776–1778.
(27) Jabbarzadeh, A.; Harrowell, P.; Tanner, R. I. Crystal bridge formation marks the transition to rigidity in a thin lubrication film. *Phys. Rev. Lett.* **2006**, *96*, 206102–1/4.
(28) Daivis, P.; Evans, D. *J. Chem. Phys.* **1992**, *97*, 616–627.
(29) Higgins, J. S. Benoît, H., *Polymers and neutron scattering*; Oxford: Oxford, U.K., 1994.
(30) Hosier, I. L.; Bassett, D. C. A study of the morphologies and growth kinetics of three monodisperse n-alkanes C_{122} H_{246}, C_{162} H_{326}, and C_{246} H_{494}. *Polymer* **2000**, *41*, 8801–8812.
(31) Jabbarzadeh, A.; Atkinson, J. D.; Tanner, R. I. Effect of molecular shape on rheological properties in molecular dynamics simulation of star, H, comb, and linear polymer melts. *Macromolecules* **2003**, *36*, 5020–5031.
(32) Moore, J. D.; Cui, S. T.; Cochran, H. D.; Cummings, P. T. A molecular dynamics study of a short-chain polyethylene melt. II. Transient response upon onset of shear. *J. Non-Newtonian Fluid Mech.* **2000**, *93*, 101–116.
(33) Pearson, D.; Herbolzheimer, E.; Grizzuti, N.; Marrucci, G. Transient behavior of entangled polymers at high shear rates. *J. Polym. Sci., Part B* **1991**, *29*, 1589–1597.
(34) Bove, L.; Nobile, M. R. Shear flow effects on polymer melts crystallization: kinetics features. *Macromol. Symp.* **2002**, *180*, 169–180.
(35) Kumaraswamy, G.; Kornfield, J. A.; Yeh, F.; Hsiao, B. S. Shear-enhanced crystallization in isotactic polypropylene. 3. Evidence for a kinetic pathway to nucleation. *Macromolecules* **2002**, *35*, 1762–1769.
(36) Balzano, L. Ph.D. Thesis. Eindhoven Uni. of Tech.: Eindhoven, The Netherlands, 2008.
(37) Tanner, R. I. *Engineering rheology*; Oxford: Oxford, U.K., 2000.